Plant Nano Biology 14 (2025) 100215

Contents lists available at ScienceDirect

Plant Nano Biology

journal homepage: www.journals.elsevier.com/plant-nano-biology

Nanomaterials for the control of the onion phytopathogen *Botrytis squamosa*

Pablo Galeano [a,b], Noheilly Vásquez [c], Helena Pardo [d], Laura Franco Fraguas [a], Guillermo A. Galván [e], Silvana Alborés [c,*]

[a] Área de Bioquímica, Departamento de Biociencias, Facultad de Química, Universidad de la República, Montevideo, Uruguay
[b] Posgrado en Química, Facultad de Química, Universidad de la República, Montevideo, Uruguay
[c] Área de Microbiología, Departamento de Biociencias, Facultad de Química, Universidad de la República, Montevideo, Uruguay
[d] Área Física & Centro NanoMat, Departamento de Experimentación y Teoría de la Estructura de la Materia y sus Aplicaciones (DETEMA), Facultad de Química, Universidad de la República, Montevideo, Uruguay
[e] Departamento de Producción Vegetal, Facultad de Agronomía, Universidad de la República, Centro Regional Sur (CRS), Progreso, Canelones, Uruguay

ARTICLE INFO

Keywords:
Allium cepa
Antifungal effects
Biogenic nanoparticles
Botrytis squamosa
Chitosan
Defense-related-enzymes

ABSTRACT

Nanomaterials can modulate plant physiology and plant–microbe interactions, offering sustainable alternatives for disease control. This study describes the synthesis and characterization of silver nanoparticles (from *Phanerochaete chrysosporium*), chitosan nanoparticles, and chitosan–silver nanohybrids, and evaluates their effects on the *Botrytis squamosa–Allium cepa* pathosystem. Silver nanoparticles were synthesized by fungal-mediated bioreduction, chitosan nanoparticles by ionic gelation, and nanohybrids by combining chitosan and silver nanoparticles. Nanomaterials were characterized by UV–visible spectroscopy, dynamic light scattering, ζ-potential, X-ray diffraction, ATR-FTIR spectroscopy, and TEM. In vitro antifungal assays, determining the effective nanomaterial concentration for 50 % inhibition of mycelial growth, demonstrated strong inhibition of *B. squamosa*, with chitosan–silver nanohybrids showing the highest activity. Controlled environment trials using *Allium cepa* (onion) whole pot plants demonstrated that chitosan nanoparticles and chitosan–silver nanohybrids reduced disease severity and induced the activity of enzymes involved in resistance mechanisms. Notably, this is the first report on the use of both chitosan-based nanomaterials in the *B. squamosa–A. cepa* pathosystem, revealing their potential to both suppress the pathogen and stimulate plant immunity. Treated plants showed increased activity of defense-related enzymes, suggesting nanoparticle-mediated priming of defense responses. These findings suggest a dual mechanism of action: direct antifungal effects and activation of plant defense responses. This work advances our understanding of nanoparticle–plant–pathogen interactions and underscores the value of biogenic nanomaterials as environmentally friendly tools for crop protection. By elucidating the biochemical responses elicited by nanomaterials, the study contributes novel insights into the molecular basis of enhanced plant resilience.

1. Introduction

The synthesis of nanoparticles can be carried out through physical and chemical methods. However, the biological or *green* fabrication of nanoparticles has become increasingly accepted due to its advantages such as environmental safety, cost-effectiveness, and scalability. Traditional methods involve high energy use, elevated temperatures, and potentially hazardous chemicals, while green fabrication eliminates such risks. Biogenic nanoparticles, such as those made from fungi, have shown promising results in agricultural and biomedical applications, including pest control and disease prevention (Khatoon et al., 2024). The effectiveness of biogenic silver nanoparticles was demonstrated in controlling early blight disease in tomatoes caused by *Alternaria solani* (Khatoon et al., 2024).

Green synthesis methods of nanoparticles using microorganisms or plant biomolecules offer an eco-friendly alternative to traditional chemical and physical nanoparticle production. The biological synthesis of nanomaterials not only reduces the use of toxic chemicals but also

Abbreviations: CHIT, chitinase activity; CS, chitosan; CSNPs, chitosan nanoparticles; CS-PchNHs, nanohybrids; Dai, days after inoculation; Dbi, days before inoculation; GLU, Glucanase activity; NPs, nanoparticles; PchNPs, biogenic silver nanoparticles; POX, Peroxidase activity.

* Corresponding author.
E-mail address: salbores@fq.edu.uy (S. Alborés).

https://doi.org/10.1016/j.plana.2025.100215
Received 30 March 2025; Received in revised form 10 July 2025; Accepted 16 October 2025
Available online 17 October 2025

improves the nanoparticle stability. Biogenic nanomaterials have shown superior efficacy in controlling plant diseases and promoting sustainable agriculture. For example, silver and magnesium oxide nanoparticles synthesized through biological methods have demonstrated strong antifungal activity, outperforming traditional chemical fungicides (Rashid et al., 2025). Moreover, biogenic selenium nanoparticles produced using fungi like *Trichoderma harzianum* have been shown to enhance the biocontrol activity against fungal pathogens, such as *Sclerotinia sclerotiorum*. Selenium nanoparticles, along with chitosan-selenium nanocomposites, have also been effective as biocontrol agents against pests like *Spodoptera littoralis*, the cotton leafworm (Ibrahiem et al., 2025). In this context, the use of fungi for the biological synthesis of silver nanoparticles represents a novel and underexplored approach. This fungal-mediated method not only harnesses the enzymatic and reducing capabilities of fungi but also aligns with the principles of sustainable agriculture by minimizing environmental impact (Sanguiñedo et al., 2023). The resulting nanoparticles exhibit enhanced antifungal activity, offering a promising alternative to conventional agrochemicals and expanding the toolkit of biologically derived nanomaterials for crop protection.

Similarly, nanochitosan, derived from chitosan (CS), has emerged as an effective antimicrobial agent, showing significant antibacterial activity against bacterial rice diseases like leaf blight and leaf spot (Wang et al., 2024). The mechanism behind nanochitosan action includes direct antibacterial effects, and the induction of resistance in plants by enhancing the activity of enzymes involved in plant defense (Wang et al., 2024). CS itself, a biopolymer with antimicrobial properties, has demonstrated activity against a broad range of pathogens, including fungi, bacteria, and viruses. Furthermore, CS has been shown to enhance plant resistance by stimulating the activity of pathogenesis-related enzymes such as peroxidases, chitinases, and glucanases, among other mechanisms (De Vega et al., 2021; Riseh et al., 2022).

Chitosan nanoparticles (CSNPs) have been utilized in various sectors such as biomedicine, food preservation, and agriculture, due to their biodegradable, low-cost, and environmentally friendly nature. CSNPs exhibit antibacterial activity by interacting with microbial cell walls, and they can also enhance plant defense mechanisms by inducing the production of pathogenesis-related enzymes (Wang et al., 2024; Akdaşçi et al., 2025).

The broad-spectrum activity of chitosan and its nanoparticles has led to their application in plant disease control, including their antifungal activity against *Alternaria* and *Rhizoctonia* species (Mohamed and Madian, 2020). Combining chitosan with other nanoparticles, such as silver, has proven to enhance their antifungal effects and offers a promising approach to integrated pest and disease management in agriculture (Vásquez et al., 2024). Recently, the potential control of *Fusarium* and *Verticillium* wilt of *Brassica napus* by a chitosan-silver nanocomposite was reported (Nawab et al., 2025).

The onion (*Allium cepa* L.) ranks as the fourth most important vegetable crop globally in terms of volume and cultivated area. It is grown on every continent. In 2023, global production reached 111 million tons of dry bulbs, cultivated on almost 6 million hectares (FAOSTAT, 2025). The crop shows two main phenological phases during the season: an initial leaf development stage characterized by an exponential growth of the plant, followed by the bulbing phase, during which the bulb forms at the base of the leaves (Brewster, 2008).

Leaf blight, caused by *Botrytis squamosa,* is a foliar disease that poses a significant challenge to onion cultivation. This disease is characterized by whitish necrotic spots on leaves and is present in onion-producing regions worldwide. Infection by *B. squamosa* is a major threat to onion yield and quality, often leading to substantial economic losses (Tanović et al., 2019; Steentjes et al., 2021). In Uruguay, leaf blight can cause the total loss of seedlings in the southern region early in the season, and affect the crop throughout its cycle in the northern region (Galván et al., 2004).

The control of fungal diseases in horticultural crops remains a significant challenge, particularly in the pursuit of economically viable production and the provision of healthy, high-quality food with minimal pesticide residues. Although chemical fungicides have been a valuable tool in disease management, their widespread use raises concerns regarding environmental impact and the health risks posed to workers and consumers. After several decades, and despite the introduction of new active ingredients, the development of resistance by pathogens has led to a decline in the effectiveness of chemical fungicides currently used in several crops; such is the case of onion (Leroux, 2007; Araújo et al., 2018). Regarding *B. squamosa*, some strains have become insensitive to some active ingredients of dicarboximide fungicides used for leaf blight control (Steentjes et al., 2021). There is increasing interest and public pressure to find alternatives to the use of pesticides. An example of this is the position taken by the European Parliament identifying Resistance Induction as a strategy to be developed for crop protection, which has renewed interest in the development of resistance inducers (Reinders et al., 2021).

In this context, the evaluation of chitosan-based nanomaterials emerges as a promising alternative for controlling onion leaf blight caused by *B. squamosa*. This study aimed to develop and assess sustainable nanomaterials—biogenic silver nanoparticles, chitosan nanoparticles, and chitosan–silver nanohybrids—for controlling *Botrytis squamosa* in onion crops. It integrated the synthesis and characterization of these nanomaterials with in vitro and greenhouse assays to evaluate their antifungal properties and their ability to activate plant defense mechanisms. For the first time, the synthesis, characterization, and antifungal activity of chitosan-based nanoparticles were explored in the *B. squamosa–Allium cepa* pathosystem. In addition to determining their antimicrobial effects, the study examined how these nanoparticles influence the host–pathogen interaction by monitoring symptom progression and defense-related enzymatic responses.

2. Materials and methods

2.1. Synthesis of nanomaterials

Biogenic silver nanoparticle synthesis (PchNPs) was carried out as described by Sanguiñedo et al. (2018). Two 90 mm diameter discs from the fungal mycelia of *Phanerochaete chrysosporium* (Pch) grown on Potato Dextrose Agar (PDA, OXOID) were taken and inoculated into 100 mL of liquid Potato Dextrose Broth (PDB, OXOID). Cultures were incubated at 28 °C with constant shaking at 150 rpm for 72 h. After incubation, fungal mycelium was obtained from the liquid culture, filtered, and washed with sterile distilled water. The wet fungal mycelia were then suspended in sterile distilled water (0.1 g/mL) and incubated under agitation at 150 rpm in an orbital shaker for 24 h. The resulting cell-free filtrate was obtained by filtering the suspension through a 0.45 μm pore-size membrane filter. The cell-free filtrate was mixed with 5 mM $AgNO_3$ (Sigma-Aldrich) and incubated in the dark, the synthesis process was monitored by measuring absorption spectra, between 250 and 800 nm, to track nanoparticle formation. Once the absorption peak stabilized, the nanoparticles were purified by centrifugation at 10.000 rpm for 10 min, washed, and stored (no more than 5 months) at 4 °C, until use (Sanguiñedo et al., 2018).

Chitosan–silver nanohybrids (CS-PchNHs) were synthesized as reported by Vásquez et al. (2024), using a CS (Sigma-Aldrich) solution (1.2 mg/mL) in 1 % acetic acid. CS solutions was prepared and kept under continuous stirring for 24 h. After this period, the biogenic PchNPs were added dropwise to the chitosan solutions (in a 1:1 vol ratio) and stirred for an additional 5 h. After synthesis, the resulting nanohybrids (CS-PchNHs) were centrifuged at 10.000 rpm for 20 min, washed three times with deionized water, and resuspended.

For the synthesis of chitosan nanoparticles (CSNPs), the optimized ionic gelation method was used, which involved preparing chitosan (CS) solutions in acetic acid and Sodium tripolyphosphate penta-basic (TPP, Sigma-Aldrich) solutions (1.6 mg/mL), as reported by Zimet et al.

(2018). The TPP solution was added drop by drop to the chitosan solution under stirring, and the pH was adjusted with NaOH, maintaining constant agitation at room temperature. After nanoparticle formation, they were separated by centrifugation (12,000 rpm for 10 min), washed twice, and resuspended in deionized water.

2.2. Characterization of nanomaterials

The formation and characterization of the synthesized nanomaterials were assessed using complementary techniques.

UV–visible spectroscopy was employed to monitor nanoparticle synthesis and stability, detecting the characteristic surface plasmon resonance (SPR) band of silver nanoparticles in the 400–450 nm range (Sanguiñedo et al., 2018). A Jenway 6715 UV/Visible spectrophotometer was employed, operating in the range of 250–800 nm.

Dynamic light scattering (DLS) and ζ-potential measurements were carried out to determine the hydrodynamic size distribution and surface charge of the nanoparticles and nanohybrids, providing information on their colloidal stability and dispersion behavior. PchNPs, CSNPs and CS-PchNHs were analyzed using dynamic light scattering (DLS) and electrophoretic light scattering (ELS), respectively, with a particle size/zeta potential analyzer. The Nano-Zetasizer from Malvern Instruments Ltd., Worcestershire, UK, was used, with samples prepared at pH 6 in deionized water and analyzed at 25°C, viscosity of 0.8872 cP, refractive index (RI) of 1.33, and a backscatter angle of 173°. Triplicate analyses were performed, and the particle size and zeta potential results were expressed as the mean ± standard deviation (SD), with data processed using Malvern Zetasizer software.

X-ray powder diffraction (XRD) analysis was performed to identify the crystalline phases present and to evaluate the structural interactions between silver nanoparticles and chitosan in the hybrid systems. Powder XRD patterns were obtained using a Rigaku Miniflex 600-C diffractometer operating in θ–2θ Bragg–Brentano geometry. The instrument was equipped with a Cu Kα radiation source (λ = 1.5419 Å), operating at 40 kV and 15 mA, and a D/teX Ultra2 1D detector. Measurements were performed in scan mode over a 2θ range of 3° to 70°, with a step size of 0.02° and a scanning speed of 20°/min. Both nanoparticles and nanohybrids were analyzed in their dry powder form.

Attenuated Total Reflectance–Fourier Transform Infrared (ATR-FTIR) spectroscopy was used to identify functional groups present in the nanomaterials and to detect interactions between the components, confirming the presence of capping agents and the formation of nanohybrids through chemical bonding. Analyses were performed using an ATR-FTIR spectrophotometer (SHIMADZU IRSpirit) equipped with a Pike Diamond/KRS-5 HS crystal plate.

For the HR-TEM analysis, the samples in ethanol 95 were completely dried and then observed with a JEOL JEM 2100 electron microscope of 200 kV acceleration voltage, using a copper grid. In addition, the elemental chemical composition was studied with an X-ray EDS probe on the surface of the NPs. Then, the sizes of the NPs were determined by image analysis using ImageJ Software.

2.3. Efficiency of treatments against B. squamosa

2.3.1. Antifungal activity in vitro

The effects of nanomaterials (PchNPs, CSNPs y CS-PchNHs) on the mycelium growth of the phytopathogen *B. squamosa* strain UR05 from the collection of Centro Regional Sur (CRS, Faculty of Agronomy, Universidad de la República) were evaluated, as previously reported (Sanguiñedo et al., 2023). Agar blocks (plugs) of fresh mycelium were punched out from the edge of the fungal colony using a sterile punch 5 mm in diameter. The plates containing Potato Dextrose Agar (PDA, BD Difco) supplemented with 1 mL of four different concentrations (two-fold dilutions) of nanomaterials, were inoculated in the center with one plug per plate. These plates were incubated for 5 days at 28 ºC. Control cultures of fungal strains grown in PDA with null nanomaterials were also included. After that period, the diameter of the mycelium was measured and compared with the control. The diameter of the mycelia growth in PDA medium (without nanomaterials) served as the control, representing the 100 % growth (0 % inhibition). The inhibition caused by each nanomaterial concentration was expressed as a percentage, comparing the fungal growth with the control. Additionally, for comparison purposes, $AgNO_3$ and CS solutions were included in the antifungal assay. The results were expressed as EC50 (the concentration that inhibits 50 % of mycelial growth) obtained by linear regression (correlation coefficient > 0.95) of the probit-transformed relative inhibition value and the log10 of the antifungal concentration (Tian et al., 2019).

2.3.2. Whole plant experiments

To produce the pathogen inoculum, mycelium of *B. squamosa* UR05 was plated on Petri dishes containing PDA (Potato-dextrose agar), and grown for 15 days at 20 ºC until sclerotia formation (Galván et al., 2003). These sclerotia were transferred to plates with moist sterile sand and incubated at 4 °C for 7 weeks until they germinated, producing mycelium and conidia. Germinated sclerotia were picked up and immersed in sterile distilled water with 0.1 % Tween 20 and shaken to release the conidial spores. The suspension was filtered with sterile gauze and a spore count was performed in a Neubauer chamber to adjust the concentration to 1×10^4 spores mL^{-1}.

Onion adult plants (*A. cepa*) variety Regia were used. In the trial of August 2023 (Trial 1), plants of 160 days from sowing were used, whereas 205 days-old plants were used in September 2023 (Trial 2). The plants were produced in seedbeds and transplanted to individual pots in a greenhouse until use.

Three days before being inoculated with the pathogen (3 dbi), the onion plants were pre-treated with one of the following three chitosan-based compounds: CS (2.4 mg/mL), CSNPs (2.4 mg/mL), CS-PchNHs (0.2 μg/mL). The control group of plants was sprayed with sterile water. In all cases, 0.1 % Tween 20 was used as an adhesive. At the time of inoculation with the pathogen, for each pretreatment, half of the plants were sprayed with a spore solution with a concentration of $1{\cdot}10^4$ spores/mL and the other half with sterile water. Thus, eight groups of plants with different treatments were obtained.

Inoculation was carried out by spraying each plant with approximately 6 mL of *B. squamosa* spore suspension covering the entire foliage. Each plant was then covered with a polypropylene bag and kept under controlled conditions in a growth chamber (17 ºC, 100 % relative humidity, 10 h of light per day) until symptom evaluation and sampling. In Trial 1, sampling was carried out 8 days after inoculation (dai). For Trial 2, samples were also taken at the time of inoculation (day 0), and 8 dai. For enzymatic analysis, samples were based on the third youngest leaf (leaf 3) of each plant. The samples were freeze-dried and stored at −20 ºC until processed for enzymatic analysis.

In Trial 1, 46 plants were used, which meant five to six replicates per treatment. In Trial 2, 68 plants were used; 20 of these were used to evaluate the effect of pre-treatments at the time of inoculation (five replicates for each pre-treatment at day 0); and 48 plants corresponded to six replicates per treatment (8 dai).

Symptom assessment was conducted 8 dai with *B. squamosa*, by estimating the percentage of necrotic tissue on the third and fourth youngest fully expanded leaves (leaves 3 and 4) of each plant (Currah and Maude, 1984). These leaves were on average 30–40 days old and showed no signs of senescence at the time of inoculation. Images of each leaf were taken and processed with the Quant v. 1.0.2 program to estimate necrotic area percentages. To establish statistically significant differences between data groups, ANOVA tests and multiple *t*-tests by the Holm-Sidak method were performed for $\alpha = 0.05$. The normal distribution and homoscedasticity of measured variables was checked by the Shapiro-Wilk test, and the Brown-Forsythe test, respectively. All tests were carried out using GraphPad Prism 8.0.2 software.

2.3.3. Defense-related enzymes

All enzymatic activities were determined for each plant from aqueous extracts of soluble proteins obtained from freeze-dried tissue of the third leaf. The aqueous extracts were obtained by abrasion maceration of the freeze-dried tissue in 50 mM acetate buffer pH 5.6. The clear supernatants of these extracts were gel filtered on PD-10 columns (Sephadex G25) and stored at −20ºC until analysis. In all cases, the enzymatic activities were determined according to the method reported by Galeano et al. (2014), and expressed in enzyme units (EU) per gram of freeze-dried tissue. Changes in enzyme activity due to different treatments were expressed as the ratio of enzyme activity in the treated samples to that in the corresponding controls. Peroxidase activity (POX) was determined using o-dianisidine as a substrate, performing the assays at room temperature and pH 4.8. The POX EU is defined as the amount of enzyme that oxidizes 1 μmol of substrate per min. under the reaction conditions. Glucanase activity (GLU) was determined using laminarin as substrate, by glucose release at 37°C, using a calibration curve with glucose. The GLU EU is defined as the amount of enzyme that releases 1 mg of reducing sugars in the form of glucose under the reaction conditions. Chitinase activity (CHIT) was measured using azure chitin as the substrate, with one CHIT EU defined as the amount of enzyme required to increase the absorbance at 560 nm by 0.01 under the specified reaction conditions (3 h, 40 ºC, pH 5.6).

All the activity assays were performed in triplicate. To establish statistically significant differences between data groups, ANOVA tests and multiple *t*-tests by the Holm-Sidak method were performed for $\alpha = 0.05$ except where indicated. The normal distribution and homoscedasticity of measured variables was checked by the Shapiro-Wilk test, and the Brown-Forsythe test, respectively. All tests were carried out using GraphPad Prism 8.0.2 software.

3. Results and discussion

3.1. Synthesis and characterization of nanomaterials

3.1.1. UV–Vis spectroscopy

The synthesis of biogenic PchNPs was performed following previous protocols from our research group, yielding reproducible results. The brown-yellowish coloration of the products suggests the formation of AgNPs, which was corroborated by UV-Vis absorption spectra, where a characteristic surface plasmon resonance (SPR) band was observed between 400 and 450 nm (Sanguiñedo et al., 2018, 2019, 2023). After the synthesis reaction begins, a band is observed at 420 nm, which corresponds to the SPR band of the PchNPs (Fig. 1A), at an estimated concentration of 0.2 μg/mL.

To combine the advantages of biogenic silver nanoparticles and CS, the synthesis of CS-PchNHs was carried out. These materials can integrate the antimicrobial properties of AgNPs with the bioactive characteristics of CS, making them attractive for sustainable agricultural applications (Chandran et al., 2024). For the case of the CS-PchNHs, the band at 416 nm was also shown in UV–vis spectrum (Fig. 1B). These results indicate the stability of both PchNPs and CSPchNHs. The obtained UV–Vis spectroscopy results were consistent with previous reports (Shahid-ul-Islam et al., 2019). Senthilkumar et al. (2019) reported the UV–Vis absorbance peak of green synthesized CS-Ag at 419 nm.

3.1.2. ζ-potential and particle size

Apart from the synthesis of PchNPs and CS-PchNHs described above, chitosan nanoparticles (CSNPs) were also synthesized in this study. The results indicated that CSNPs had a zeta potential of $+28.9 \pm 4.8$ mV, indicating a positive surface charge. Besides that, the zeta potential value of the PchNPs, and CS-PchNHs was -21.1 ± 9.1 and $+24.4 \pm 5.2$ mV, respectively, suggesting colloidal stability for all the synthesized nanomaterials (Vásquez et al., 2024).

DLS measurements were performed to determine the hydrodynamic size of the nanomaterials (Fig. 2). CSNPs showed an average size of

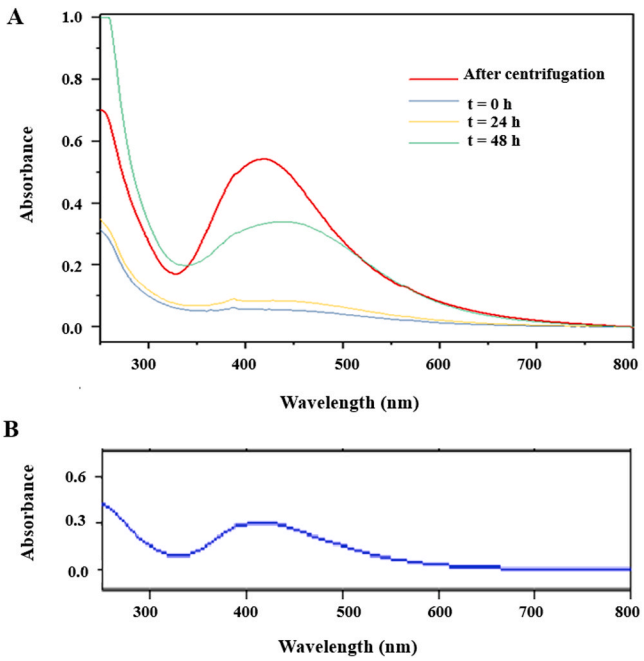

Fig. 1. UV–vis absorption spectra. **A**. Synthesis (0–48 h) and purified PchNPs. **B**. CS-PchNHs.

96.6 nm and a narrow size distribution, with a PDI of 0.1, suggesting high homogeneity in the final sample. These findings align with those reported by Winayu et al. (2019), who demonstrated that a lower acetic acid concentration influences the size of CSNPs. In this context, acetic acid is used to protonate the amino groups of CS, facilitating interaction with the negative charges of TPP and promoting the formation of smaller nanoparticles. However, high concentrations may induce agglomeration, making it crucial to optimize the synthesis reaction of CSNPs (Winayu et al., 2019).

The average hydrodynamic diameters of PchNPs was 22 nm, with a 0.2 polydispersity index (PDI) value. For the nanohybrid system CS-PchNHs, the particle diameters were 143.6 nm and PDI 0.4. In nanoparticle synthesis, PDI values below 0.3 are generally preferred, higher PDI values suggest a broader size distribution, often associated with aggregation (Jampafuang et al., 2019).

Compared to previous studies, the characteristics of the biogenic PchNPs and CS-PchNHs are consistent with other fungal-based silver nanoparticles, which typically present SPR peaks around 420 nm and similar zeta potential values. However, the CS-PchNHs developed here exhibited a more controlled particle size and better colloidal stability than some previously reported CS-Ag systems, such as those from Stereum hirsutum and Aspergillus fumigatus, where larger sizes and higher PDI values were observed (Raza et al., 2021; Hermosilla et al., 2023). These results highlight the relevance of optimizing synthesis conditions to obtain stable nanomaterials with potential applications in agriculture, where both antimicrobial activity and biocompatibility are essential. The combination of chitosan and biogenic silver nanoparticles results in a promising nanohybrid material with improved colloidal behavior compared to uncoated AgNPs, supporting its application as an eco-friendly alternative in plant disease management.

3.1.3. Transmission electron microscopy

TEM images (Fig. 3) reveal the presence of spherical nanoparticles. The average size of the CS-PchNHs was 65 ± 35 nm, smaller than those reported by DLS, which is expected since the DLS measures the hydrodynamic diameter of the particles. Energy Dispersive Spectroscopy analysis confirmed the presence of silver nanoparticles and chitosan in the CS-PchNHs, as indicated by the silver and nitrogen peaks, supporting

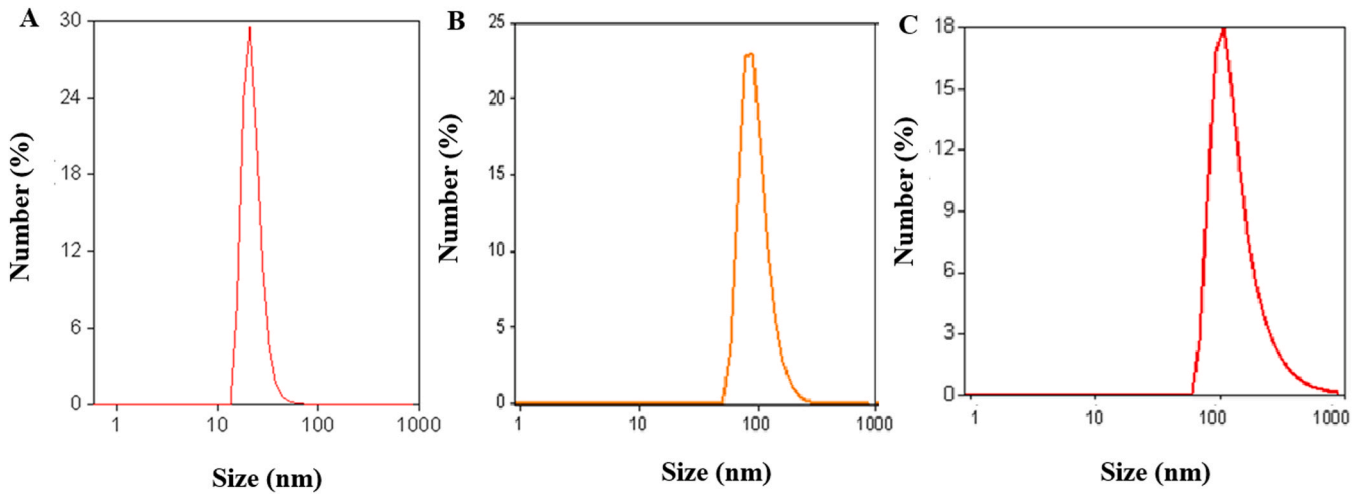

Fig. 2. Characterization of the three studied nanomaterials diameters by DLS **A.** PchNPs **B**,CSNPs, **C.** CS-PchNHs.

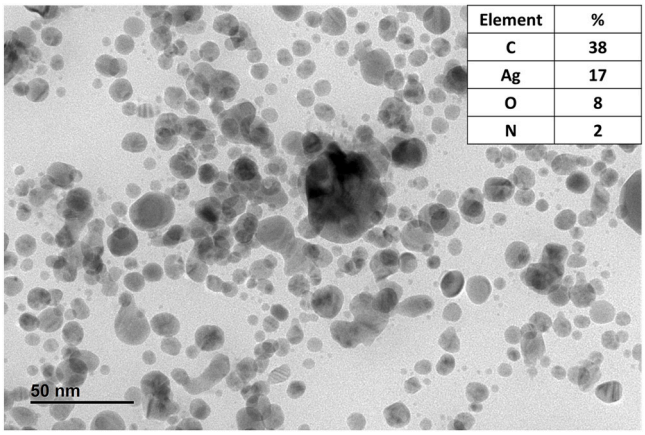

Element	%
C	38
Ag	17
O	8
N	2

Fig. 3. TEM image and EDS spectral analysis of CS-PchNHs.

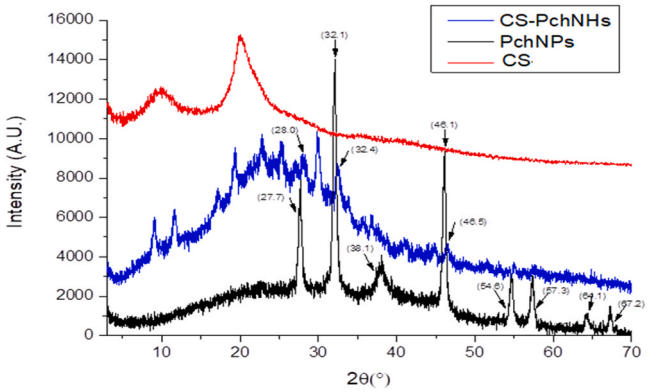

Fig. 4. XRD patterns of biogenic silver nanoparticles (PchNPs), chitosan-Ag nanohybrids (CS-PchNHs), and chitosan, shown from bottom to top, respectively.

previous reports of similar nanohybrid compositions (Tharani et al., 2020). The detection of other peaks could be attributed to the organic phase of the CS and the biogenic NPs (Bharathi et al., 2018, Sanguiñedo et al., 2023). The percentages of the principal elements present in the NHPch were also included in Fig. 3.

3.1.4. *X-ray powder diffraction*

As described by Vásquez et al. (2024), the X-ray powder diffraction -XRD- analysis of the chitosan–silver nanohybrids (CS-PchNHs) showed an increase in the amorphous background and a reduction in chitosan crystallinity, suggesting that the incorporation of negatively charged biogenic silver nanoparticles (PchNPs) introduces structural disorder, indicative of ionic cross-linking interactions between chitosan and the silver nanoparticles. Additionally, as can be observed in Fig. 4, the comparison between the diffraction patterns of PchNPs and CS-PchNHs revealed the presence of characteristic silver peaks—particularly those around $2\theta = 32°$, 38°, and 46° (Senthilkumar et al., 2019), associated with metallic silver (Ag^0)—confirming the successful incorporation of the nanoparticles into the hybrid structure. Other reflections observed in the PchNPs pattern likely originate from crystalline components of the organic capping agents, and are also retained in the CS-PchNHs diffractogram.

3.1.5. *Attenuated total reflectance–fourier transform infrared (ATR-FTIR) spectroscopy*

The ATR-FTIR spectrum of PchNPs revealed distinct vibrational features indicative of their chemical composition and surface functionalization (Fig. 5). Protein-related functional groups were confirmed by peaks at 564.48 cm^{-1} (amide II deformation) and 1539.76 cm^{-1} (amide I stretching), associated with C–N–H and C═O bonds (Ballottin et al., 2016; Parmar et al., 2019). Additional protein signals include bands at 623.37 cm^{-1} and 1317.13 cm^{-1} , attributed to primary amine bending and asymmetric stretching, respectively (Guilger-Casagrande et al., 2021; Jyoti et al., 2016; Parmar et al., 2019). Polysaccharide presence was evidenced by a strong band at 1026.99 cm^{-1} , corresponding to symmetric C–O–C glycosidic bond stretching in the pyranose ring (Ahluwalia et al., 2014; Priya et al., 2020). Aliphatic CH_2 and CH_3 groups were identified at 2878.44, 2915.79, and 1376.02 cm^{-1} (Guilger-Casagrande et al., 2021; Li et al., 2018), while N–H (3294.98 cm^{-1}) and O–H (3410.65 cm^{-1}) stretching vibrations indicated the presence of amide and hydroxyl groups (Ahluwalia et al., 2014; Jyoti et al., 2016).

The ATR-FTIR spectrum of CS-PchNHs confirmed the successful formation of the hybrid material through the coexistence of characteristic signals from both chitosan and silver nanoparticles (Fig. 5). The presence of Ag–O vibrations at 511.34 and 639.17 cm^{-1} confirmed the incorporation of biogenic silver nanoparticles into the hybrid matrix (Alamri et al., 2018; Guilger-Casagrande et al., 2021). Key structural features of chitosan were retained, as indicated by the presence of C–O–C glycosidic stretching bands at 1018.37, 1025.55, and 1026.99 cm^{-1} , and aromatic C–H bending at 801.48 cm^{-1} (Sullivan et al., 2018). Evidence of interaction between CS and PchNPs was

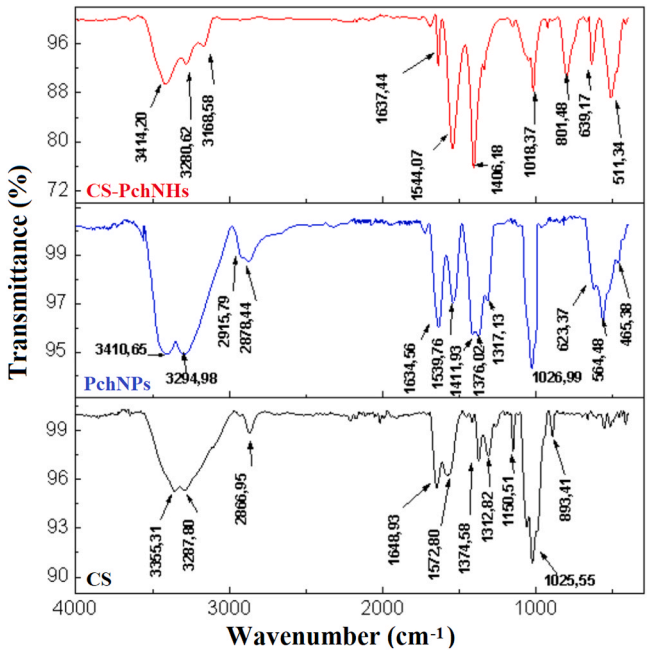

Fig. 5. ATR-FTIR spectra of chitosan, biogenic silver nanoparticles (PchNPs) and chitosan–Ag nanohybrids (CS-PchNHs), shown from bottom to top, respectively.

supported by shifts in several characteristic bands. The aromatic C–O–C band of PchNPs shifted from 1411.93 cm^{-1} to 1406.18 cm^{-1} in the CS-PchNHs. N–H stretching bands from CS (1572.80 cm^{-1}) and PchNPs (1539.76 cm^{-1}) emerged into a single peak at 1544.07 cm^{-1} in CS-PchNHs. Similarly, the amide C═O band of CS shifted from 1648.93 cm^{-1} to 1637.44 cm^{-1} , while the corresponding PchNPs band at 1634.56 cm^{-1} was also affected. Finally, O–H stretching bands from CS (3287.80 cm^{-1}) and PchNPs (3294.98 and 3410.65 cm^{-1}) shifted to 3168.58 and 3280.62 cm^{-1} , respectively, in the spectrum of the CS-PchNHs.

Altogether, the FTIR analysis provides strong evidence for the successful formation of CS-PchNHs and suggests that the interaction between chitosan and biogenic silver nanoparticles involves multiple functional groups, including Ag–O, N–H, amide, and hydroxyl groups.

3.2. Efficiency of treatments against B. squamosa

3.2.1. Antifungal activity in vitro

In vitro antifungal activity of synthesized nanomaterials against *B. squamosa* was evaluated (Table 1). PchNPs and CS-PchNHs, showed *in vitro* inhibition on fungal growth, but not CSNPs (Supplementary Material-Fig.SM1). Although $AgNO_3$ and CS solutions also inhibited mycelia growth, these two treatments showed very higher EC50 values, suggesting low antifungal activity. The EC50 values of the nanomaterials that inhibited fungal growth were very low, demonstrating their potential application for the direct control of *B. squamosa* in plants. Furthermore, CS-PchNHs showed the highest antifungal activity among the evaluated materials (EC50 0.21 μg/mL) suggesting a possible synergy between their components.

Table 1
Inhibitory effect of nanomaterials on the growth of *B. squamosa* mycelium.

Treatments	Toxicity regression equation	EC_{50}(μg/mL)	Correlation coefficient
CS	y = 0,9567x + 4,5405	3020	0,9938
$AgNO_3$	y = 0,6445x + 3,3885	317	0,9827
PchNPs	y = 1,8885x + 5395	0,47	0,9997
CS-PchNHs	y = 1,7606x + 6,2	0,21	0,9666

The high performance of PchNPs and nanohybrids could be related to various physicochemical properties of the materials. Characteristics such as surface charge and particle size influence their interaction with fungal cells. It has been proposed that the higher positive charge of nanohybrids facilitates their interaction with the negative charge of fungal cell membranes, causing structural alterations (Barabadi et al., 2020; Kulikouskaya et al., 2022; Mondéjar-López et al., 2023; Vásquez et al., 2024). Kulikouskaya et al. (2022) suggested that the electrostatic attraction between positively charged nanomaterials and negatively charged microbial cells is a key factor in their antimicrobial activity. Additionally, the binding of CS to the microbial cell wall may alter its structure and enhance the antimicrobial efficacy of nanocomposites.

Indeed, another possible mechanism of action of PchNPs involves their interaction with the cell membrane, altering its permeability, integrity, and respiratory functions. The alteration of membrane permeability under the action of CS-silver nanoparticles could facilitate their penetration into the microbial cell, resulting in an enhanced antimicrobial effect (Kulikouskaya et al., 2022). However, not all evaluated materials exhibited the same behavior. In the case of the CSNPs synthesized in this study, no inhibition of phytopathogen growth was observed under the evaluated conditions.

This lack of *in vitro* antifungal activity of CSNPs could be due to multiple factors, including the intrinsic characteristics of CS (e.g., its molecular weight) or the specific properties of the synthesized CSNPs (e.g., their surface charge). In particular, the measured Z potential values for CSNPs were approximately + 20 mV, lower than those reported in the literature, which could indicate a weaker interaction with fungal cells (Kheiri et al., 2016). These results highlight the importance of optimizing the physicochemical properties of nanomaterials to maximize their antifungal effectiveness.

3.2.2. Evaluation of symptoms in onion plants caused by B.squamosa

Symptom evaluation was performed by estimating the percentage of necrotic tissue in leaves 3 and 4 of each plant, 8 dai with *B. squamosa*, as described in Methods. In both trials, the plants treated (3 dbi) with the different compounds (CS, CSNPs, CS-PchNHs), but not inoculated with the pathogen, did not develop necrotic spots (Supplementary Material-Fig.SM2). Table 2 presents the percentage of affected leaf area in leaves 3 and 4 across both trials for treatments in which plants were inoculated with the pathogen. As an illustration, Fig. 6 shows representative symptoms on the 3rd leaf of plants from Trial 2.

For both trials, the chitosan-based nanomaterials reduced the symptoms caused by the pathogen 8 dai when treating the plants 3 dbi. The differences were statistically significant when comparing the groups of plants pretreated with those inoculated without pretreatment (+*B. sq.*). Similar results were obtained in the CS pretreatments, with the exception of the evaluation of leaf 4 in trial 1, in which case the reduction was not statistically significant. Although the CS-PchNHs treatment was applied at a much lower concentration than CS and CSNPs, its inclusion was based on the known high efficacy of silver nanoparticles at low doses and the anticipated synergistic effect between chitosan and PchNPs, which allows for effective protection with reduced material input.

Furthermore, a statistical comparison of both trials (two way ANOVA, Holm-Sidak multiple comparisons test, Supplementary Material-Fig.SM3) reveals that reduction of symptoms was significantly greater in Trial 2 than in Trial 1, regardless of the leaf evaluated. In Trial 1, the average symptom reduction explained by the chitosan-based compounds was 53 % and 54 % for leaf 3 and leaf 4, respectively, whereas in Trial 2, these values increased to 76 % and 75 %. The difference between the trials may be related to the distinct phenological stage of the plants, as plants had begun to bulb in Trial 2 at the time of inoculation. Onion bulbing phase is triggered by long days, dealing to changes in gene expression and hormonal ratios (Lee et al., 2013). These findings suggest that the effectiveness of these compounds in enhancing

Table 2
Percentage of onion leaf area affected by *B. squamosa (B.sq)* on leaves of *Allium cepa* var. 'Regia'.

Treatment	Trial 1				Trial 2			
	Leaf 3		Leaf 4		Leaf 3		Leaf 4	
	%	SD	%	SD	%	SD	%	SD
+*B.sq*	2.6[a]	0.6	4.8[a]	1.7	2.1[a]	1.0	3.4[a]	3.0
CS +*B.sq*	1.2[b]	0.7	3.0[ab]	1.7	0.6[b]	0.4	0.8[b]	0.4
CSNPs +*B.sq*	1.4[b]	0.8	1.6[b]	1.5	0.4[b]	0.2	1.0[b]	0.3
CS-PchNHs +*B.sq*	1.0[b]	0.6	1.9[b]	0.9	0.6[b]	0.3	1.0[b]	1.0

SD: standard deviation
Within each column, different letters after the mean values indicate significant differences between treatments ($p \leq 0.05$).

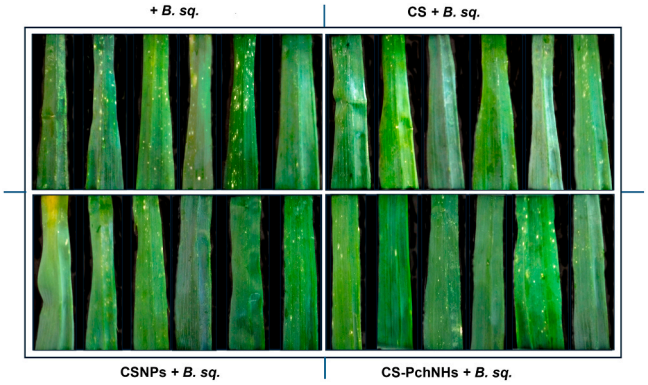

Fig. 6. Symptoms in the 3rd leaf of onion plants (var. Regia) 8 days after inoculation with *B. squamosa*. The chitosan-based compounds with which the plants were treated 3 days before inoculation are indicated. The images shown correspond to Trial 2.

onion defense against *B. squamosa* might be influenced by the plant's phenological stage.

For several plant-pathogen interactions, it is known that plant resistance changes according to its stage of development. This phenomenon is called age-associated resistance and manifests itself at different times depending on the pathosystem under study (Panter and Jones, 2002; Develey-Rivière and Galiana, 2007). In our study, onion resistance to *B. squamosa* was not influenced by plant age; however, changes in the impact of chitosan-based compounds on the plant's defense response were observed.

3.2.3. *Defense-related enzymes*

Chitosan is known to confer a dual benefit by exhibiting antimicrobial activity and inducing plant resistance. The induced resistance state is characterized by the activation of latent defense mechanisms that are induced early after induction, and with greater intensity in the event of a subsequent attack by a pathogen in a phenomenon called 'priming'(Pieterse et al., 2014; Martinez-Medina et al., 2016). *Priming* can be induced by various factors, such as treatment with chitosan-based compounds evaluated in this study.

Then, to assess whether the tested chitosan-based nanomaterials elicit resistance in the selected pathosystem, we analyzed the activities of pathogenesis-related enzymes (PRs) in response to different treatments. Several chitinases, glucanases and peroxidases have been classified as PRs since they are induced in the early stages of plant-pathogen interaction (Dos Santos and Franco., 2023; Han and Schneiter, 2024). Furthermore, several studies have reported that chitosan-induced resistance is associated with increased activity of those enzymes (Román-Doval et al., 2023).

In Trial 2, prior to inoculation with *B. squamosa*, samples were taken from the third leaf of pretreated plants with the different chitosan-based compounds. Sampling was done before inoculation with the pathogen, three days after treating the plants with these compounds in order to determine whether enzymatic activities were altered and can be linked to differences in the subsequent development of disease symptoms once the plants are inoculated with the pathogen.

The results showed significant changes in some enzymatic activities due to the treatments (Table 3, Supplementary Material-Fig.SM4). As expected, CHIT activity increased in response to all chitosan treatments, although this increase was statistically significant only in plants treated with CS-PchNHs ($p \leq 0.1$). On the other hand, POX activity decreased. Although it was an unexpected result, there are reports that different factors such as a high CS concentration, can inhibit POX activity (Shams Peykani and Farzami Sepehr, 2018). No significant variations were observed in GLU activity with the treatments.

Furthermore, the enzymatic activities eight dai with *B. squamosa* were evaluated from the third leaf of the treated plants. In both trials carried out, it was studied whether changes in the activity of the evaluated enzymes occur in plants inoculated with the pathogen and whether these changes are linked to pretreatment with the different chitosan-based compounds. Results comparing symptoms and enzymatic activity ratio (EU/g plants inoculated: EU/g plants not inoculated) are shown in Fig. 7.

For non-inoculated plants, no differences were detected in these activities between plants pretreated with the chitosan-based compounds and those pretreated with water (controls). This means that the changes in CHIT and POX activities observed three days after treating the plants with the chitosan-based compounds were transient, since they were not observed eight days later.

Inoculation with the pathogen produced a significant increase in POX activity in plants that were not pretreated with chitosan-based compounds. These plants showed the highest levels of symptoms and POX activity increased 2.2 and 2.4 times in Trial 1 and 2 respectively. In plants pretreated with CSNPs and CS-PchNHs, pathogen inoculation produced a significant raise in POX activity in both trials, increasing 2.4 and 1.4 times for CSNPs, and 2.2 and 1.6 times for CS-PchNHs. It is

Table 3
Enzymatic activities three days after treatment of onion plants with chitosan-based compounds, for peroxidases (POX) and chitinases (CHIT).

Treatment	POX		CHIT	
	UE/g	SD	UE/gr	SD
Control	23[a]	2.6	158[a*]	31
CS	16[b]	3.4	204[ab*]	61
CSNPs	18[b]	3.8	198[ab*]	53
CS-PchNHs	14[b]	3.4	251[b*]	90

SD: standard deviation
Within each column, different letters after mean values indicate significant differences between treatments ($p \leq 0.05$, $*p \leq 0.1$).
Figure legends

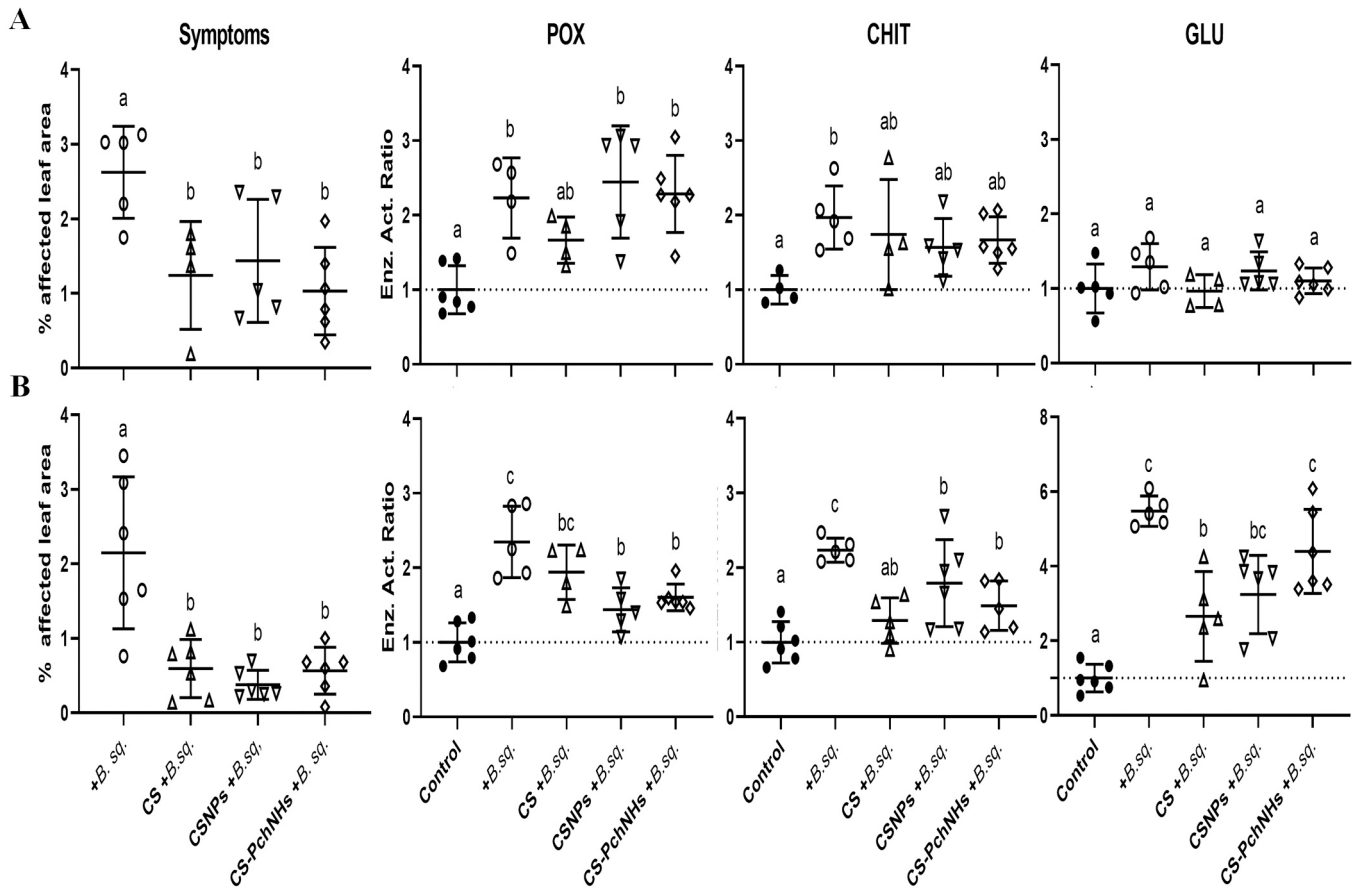

Fig. 7. Symptoms and enzymatic activity ratio (3rd leaf, 8 dai). A: Trial 1; B: Trial 2. Treatments: Control, uninoculated; +B.sq., inoculated; CS, CSNPs and CS-PchNHs indicate the pre-treatment. Different letters indicate significant differences between treatments ($p \leq 0.05$).

noteworthy that, for Trial 1, while these compounds reduce symptoms by about half, POX activity increases in the same proportion as in non-pretreated plants. In Trial 2, these plants showed a more drastic reduction of symptoms (around 75 %) and presented a smaller increase in POX activity than the plants inoculated without pretreatment. However, these increases were still significant in relation to the no inoculated plants. In plants pretreated with Chitosan, POX activity did not increase significantly in the inoculated plants in Trial 1 but this activity nearly doubled in Trial 2. These results show that POX activity increases with increasing damage caused by the pathogen, but it plays a role in its containment in plants pretreated with CSNPs and CS-PchNHs. In the case of chitosan, the results are ambiguous, but it should be noted that the phenological state of the plants was different in each trial, so they could respond differently to treatment with this compound.

Regarding CHIT activity, inoculation with the pathogen produced a significant increase in this activity in plants that were not pretreated with chitosan-based compounds, in both trials (2.0 and 2.2 times in Trial 1 and 2 respectively). In Trial 1 the increases in CHIT activity in inoculated pretreated plants were not statistically significant related to the control. However, these increases were similar to those of plants inoculated without pretreatment, although somewhat lower (1.7, 1.6 and 1.7 times for inoculated plants pretreated with, CS, CSNPs and CS-PchNHs respectively). In Trial 2, despite having developed fewer symptoms, plants pretreated with nanomaterials showed statistically significant increases over the control, increasing 1.8 for CSNPs and 1.5 for CS-PchNHs. These results show that CHIT activity increases in response to damage caused by the pathogen, but plays a role in its containment in plants pretreated with CSNPs and CS-PchNHs.

Regarding GLU activity, in Trial 1, inoculation with the pathogen did not produce significant increases in this activity in the plants for any treatment. On the other hand, in Trial 2, inoculation produced an increase in this activity for all treatments. The most notable difference between the two trials is the reduced basal GLU activity in the non-inoculated treatments of Trial 2 (6.4 UE/g) compared to Trial 1 (39 UE/g), likely due to differences in the plants' phenological stages, as previously mentioned. For Trial 2, the greatest increase was observed in plants without prior treatment, with GLU activity increased 5.5 times. Among the plants pretreated with chitosan-based compounds, the greatest increase was observed in those treated with CS-PchNHs (4.4 times), followed by CSNPs (3.2 times), and CS (2.7 times). These results show that GLU activity increases in response to damage caused by the pathogen, but it plays a role in its containment in plants pretreated with the compounds tested, particularly the CS-PchNHs. Apparently, the role of this enzyme in the response to the pathogen and in the induced resistance is dependent on the phenological state of the plant.

Taken together, these results indicate that disease development leads to the highest increases in the evaluated enzyme activities, reflecting a defense response that is ultimately insufficient to halt pathogen progression. In contrast, pretreatment with chitosan-based compounds reduces symptom development, suggesting that these compounds act either directly through antimicrobial activity or indirectly by inducing plant defense mechanisms. Notably, although CSNPs did not exhibit direct antifungal activity against *B. squamosa*, they were equally effective in reducing symptoms as the other compounds. This supports the hypothesis that resistance induction plays a key role in the protective effect of the tested compounds.

The increase in enzyme activities in response to the pathogen in pretreated plants, despite reduced symptom development, suggests that these enzymes are involved in the defense mechanisms induced by the chitosan-based compounds. The differing effects of pretreatments

observed between the two trials underscore the influence of the plant's phenological stage on the response. In Trial 1, when plants had not yet initiated bulbing, the pretreatments primarily led to increased POX activity, with this effect being more pronounced for the nanocomposites. In Trial 2, as plants began to bulb, the responses were more robust and involved all three enzymes, with nanohybrids notably enhancing GLU activity. Although symptom reduction was comparable between chitosan and nanoparticle treatments, the overall increase in enzyme activity was generally lower in plants treated with chitosan alone compared to those treated with nanocomposite formulations.

4. Conclusions

This study successfully synthesized and characterized biogenic silver nanoparticles, chitosan nanoparticles, and chitosan-silver nanohybrids. In vitro assays showed that PchNPs and CS-PchNHs had strong antifungal activity against *Botrytis squamosa*, with CS-PchNHs displaying synergistic effects. Growth chamber trials demonstrated that chitosan-based treatments reduced disease symptoms in onion plants, especially during bulb formation. Enhanced enzymatic responses, particularly peroxidase activity, in treated plants suggest these materials prime plant defenses, mitigating disease severity. Overall, CS-PchNHs emerge as a promising, sustainable strategy for managing B. squamosa, combining antifungal action and plant defense stimulation. Future work should focus on field-scale validation and integration into crop protection practices.

CRediT authorship contribution statement

Helena Pardo: Writing – review & editing, Supervision. **Galvan Guillermo:** Writing – review & editing, Supervision. **Laura Franco Fraguas:** Writing – review & editing, Supervision. **Silvana Alborés:** Writing – review & editing, Writing – original draft, Supervision, Resources, Funding acquisition, Conceptualization. **Vasquez Noheilly:** Writing – review & editing, Writing – original draft, Methodology, Formal analysis, Data curation. **Pablo Galeano:** Writing – review & editing, Writing – original draft, Methodology, Formal analysis, Data curation.

Funding

This study was funded by the Program for the Development of Basic Sciences (PEDECIBA), the National Agency for Research and Innovation (ANII-Project FMV_1_2021_1_167206) and Universidad de la República, Uruguay.

Declaration of Competing Interest

The authors declare that they have no known competing financial interests or personal relationships that could have appeared to influence the work reported in this paper.

Acknowledgments

The authors gratefully acknowledge, Dr. Belen Estevez, Dr. Iris Miraballes, Valeria Elizalde (Facultad de Química, Udelar) and Rosio Acosta, Natalia Curbelo (Centro Regional Sur, Udelar), for technical support.

Appendix A. Supporting information

Supplementary data associated with this article can be found in the online version at doi:10.1016/j.plana.2025.100215.

Data availability

Data will be made available on request.

References

Ahluwalia, V., Kumar, J., Sisodia, R., Shakil, N.A., Walia, S., 2014. Green synthesis of silver nanoparticles by trichoderma harzianum and their bio-efficacy evaluation against staphylococcus aureus and klebsiella pneumonia. Ind. Crops Prod. 55, 202–206. https://doi.org/10.1016/J.INDCROP.2014.01.026.

Akdaşçi, E., Duman, H., Eker, F., Bechelany, M., Karav, S., 2025. Chitosan and its nanoparticles: a multifaceted approach to antibacterial applications. Nanomaterials 15 (2), 126. https://doi.org/10.3390/NANO15020126.

Alamri, S.A.M., Hashem, M., Nafady, N.A., Sayed, M.A., Alshehri, A.M., Alshaboury, G., 2018. Controllable biogenic synthesis of intracellular silver/silver chloride nanoparticles by meyerozyma guilliermondii KX008616. J. Microbiol. Biotechnol. 28 (6), 917–930. https://doi.org/10.4014/JMB.1802.02010.

Araújo, E.R., Alves, D.P., Higashikawa, F.S., 2018. Cultivar resistance and chemical, biological and fertilizer treatments for controlling botrytis leaf blight of onion. Trop. Plant Pathol. 43 (2), 160–164. https://doi.org/10.1007/s40858-017-0193-x.

Ballottin, D., Fulaz, S., Souza, M.L., Corio, P., Rodrigues, A.G., Souza, A.O., Gaspari, P.M., Gomes, A.F., Gozzo, F., Tasic, L., 2016. Elucidating protein involvement in the stabilization of the biogenic silver nanoparticles. Nanoscale Res. Lett. 11 (1). https://doi.org/10.1186/s11671-016-1538-y.

Barabadi, H., Vahidi, H., Damavandi Kamali, K., Rashedi, M., Saravanan, M., 2020. Antineoplastic biogenic silver nanomaterials to combat cervical cancer: a novel approach in cancer therapeutics. J. Clust. Sci. 31 (4), 659–672. https://doi.org/10.1007/S10876-019-01697-3.

Bharathi, D., Diviya Josebin, M., Vasantharaj, S., et al., 2018. Biosynthesis of silver nanoparticles using stem bark extracts of diospyros Montana and their antioxidant and antibacterial activities. J. Nanostruct. Chem. 8, 83–92. https://doi.org/10.1007/s40097-018-0256-7.

Brewster, J.L., 2008. Physiology of crop growth, development and yield. In: Brewster, J. L. (Ed.), Onion and other Allium crops, 2nd ed. CABI Publishing, pp. 85–170.

Chandran, S., Pricillia, A., Natarajan, A., et al., 2024. Enhancing sustainability: chitosan biopolymers with ag nanoparticles for eco-friendly applications in food packaging. Biomass.. Conv. Bioref. https://doi-org.proxy.timbo.org.uy/10.1007/s13399-024-05325-7.

Currah, L., Maude, R.B., 1984. Laboratory tests for leaf resistance to botrytis squamosa in onions. Ann. Appl. Biol. 105, 277–283. https://doi.org/10.1111/j.1744-7348.1984.tb03051.x.

De Vega, D., Holden, N., Hedley, P.E., Morris, J., Luna, E., Newton, A., 2021. Chitosan primes plant defence mechanisms against botrytis cinerea, including expression of Avr9/Cf-9 rapidly elicited genes. Plant Cell Environ. 44 (1), 290. https://doi.org/10.1111/PCE.13921.

Develey-Rivière, M.P., Galiana, E., 2007. Resistance to pathogens and host developmental stage: a multifaceted relationship within the plant kingdom. N. Phytol. 175 (3), 405–416. https://doi.org/10.1111/j.1469-8137.2007.02130.x.

Dos Santos, C., Franco, O.L., 2023. Pathogenesis-Related proteins (PRs) with enzyme activity activating plant defense responses. Plants 12 (11), 2226. https://doi.org/10.3390/plants12112226.

FAOSTAT, 'Food and Agriculture Organization', Roma, Italia. Accessed: May. 08, 2025. [Online]. Available: ⟨https://www.fao.org/faostat/es/#data/QCL⟩.

Galeano, P., Gonzalez, P.H., Frano Fraguas, L., Galván, G., 2014. Age-related resistance to fusarium oxysporum f. Sp. cepae and associated enzymatic changes in seedlings of allium cepa and A. Fistulosum. Trop. Plant Pathol. 39 (5), 374–383. https://doi.org/10.1590/S1982-56762014000500004.

Galván, G., González P.H.; Reggio A. 2004. Onion leaf blight caused by Botrytis squamosa in Uruguay and the differential response of local cultivars. Allium Improvement Newsletter 13:51-54. Wisconsin, USA. ⟨https://www.ars.usda.gov/midwest-area/madison-wi/vegetable-crops-research/docs/newsletter-allium/#vol13⟩.

Guilger-Casagrande, M., Germano-Costa, T., Bilesky-José, N., Pasquoto-Stigliani, T., Carvalho, L., Fraceto, L.F., de Lima, R., 2021. Influence of the capping of biogenic silver nanoparticles on their toxicity and mechanism of action towards sclerotinia sclerotiorum. J. Nanobiotechnology. https://doi.org/10.1186/S12951-021-00797-5.

Han, Z., Schneiter, R., 2024. Dual functionality of pathogenesis-related proteins: defensive role in plants versus immunosuppressive role in pathogens. Front Plant Sci. 15, 1368467. https://doi.org/10.3389/fpls.2024.1368467.

Hermosilla, E., Díaz, M., Vera, J., Contreras, M.J., Leal, K., Salazar, R., Barrientos, L., Tortella, G., Rubilar, O., 2023. Synthesis of antimicrobial Chitosan-Silver nanoparticles mediated by reusable chitosan fungal beads. Int. J. Mol. Sci. 24 (3), 2318. https://doi.org/10.3390/IJMS24032318.

Ibrahiem, S.A., Reda, F.M., Abd-ElAzeem, E.M., Hashem, M.S., Ammar, H.A., 2025. Mycosynthesis of chitosan-selenium nanocomposite and its activity as an insecticide against the cotton leafworm spodoptera littoralis. Sci. Rep. 15 (1), 1–18. https://doi.org/10.1038/s41598-024-81988-6.

Jampafuang, Y., Tongta, A., Waiprib, Y., 2019. Impact of crystalline structural differences Between alfa- and beta-Chitosan on their nanoparticle formation via ionic gelation and superoxide radical scavenging activities. Polymers 11 (12), 2010. https://doi.org/10.3390/POLYM11122010.

Jyoti, K., Baunthiyal, M., Singh, A., 2016. Characterization of silver nanoparticles synthesized using urtica dioica linn. Leaves and their synergistic effects with

antibiotics. J. Radiat. Res. Appl. Sci. 9 (3), 217–227. https://doi.org/10.1016/J.JRRAS.2015.10.002.
Khatoon, J., Mehmood, A., Khalid, A. ur R., Khan, M.A.R., Ahmad, K.S., Amjad, M.S., Bashir, U., Raffi, M., Proćków, J., 2024. Green-fabricated silver nanoparticles from quercus incana leaf extract to control the early blight of tomatoes caused by alternaria solani. BMC Plant Biol. 24 (1), 1–10. https://doi.org/10.1186/S12870-024-05008-5/TABLES/2.
Kheiri, A., Moosawi Jorf, S.A., Mallihipour, A., Saremi, H., Nikkhah, M., 2016. Application of chitosan and chitosan nanoparticles for the control of fusarium head blight of wheat (Fusarium graminearum) in vitro and greenhouse. Int. J. Biol. Macromol. 93, 1261–1272. https://doi.org/10.1016/J.IJBIOMAC.2016.09.072.
Kulikouskaya, V., Hileuskaya, K., Kraskouski, A., Kozerozhets, I., Stepanova, E., Kuzminski, I., You, L., Agabekov, V., 2022. Chitosan-capped silver nanoparticles: a comprehensive study of polymer molecular weight effect on the reaction kinetic, physicochemical properties, and synergetic antibacterial potential. SPE Polym. 3 (2), 77–90. https://doi.org/10.1002/PLS2.10069.
Lee, R., Baldwin, S., Kenel, F., et al., 2013. FLOWERING LOCUS t genes control onion bulb formation and flowering. Nat. Commun. 4, 2884. https://doi.org/10.1038/ncomms3884.
Leroux, P., 2007. Chemical control of botrytis and its resistance to chemical fungicides. Botrytis Biol. Pathol. Control 195–222. https://doi.org/10.1007/978-1-4020-2626-3_12.
Li, H., Huang, J., Lu, F., Liu, Y., Song, Y., Sun, Y., Zhong, J., Huang, H., Wang, Y., Li, S., Lifshitz, Y., Lee, S.T., Kang, Z., 2018. Impacts of carbon dots on rice plants: boosting the growth and improving the disease resistance. ACS Appl. Bio Mater. 1 (3), 663–672. https://doi.org/10.1021/ACSABM.8B00345/.
Martinez-Medina, A., Flors, V., Heil, M., Mauch-Mani, B., Pieterse, C.M.J., Pozo, M.J., Ton, J., van Dam, N.M., Conrath, U., 2016. Recognizing plant defense priming. Trends Plant Sci. 21 (10), 818–822. https://doi.org/10.1016/j.tplants.2016.07.009.
Mohamed, N., Madian, N.G., 2020. Evaluation of the mechanical, physical and antimicrobial properties of chitosan thin films doped with greenly synthesized silver nanoparticles. Mater. Today Commun. 25, 101372. https://doi.org/10.1016/J.MTCOMM.2020.101372.
Mondéjar-López, M., López-Jimenez, A.J., Ahrazem, O., Gómez-Gómez, L., Niza, E., 2023. Chitosan coated - biogenic silver nanoparticles from wheat residues as Green antifungal and nanoprimig in wheat seeds. Int. J. Biol. Macromol. 225, 964–973. https://doi.org/10.1016/J.IJBIOMAC.2022.11.159.
Nawab, R., Akbar, M., Anar, M., Chaudhary, H.J., Hussain Munis, M.F., 2025. Biocatalytic application of chitosan-silver nanocomposite (Ch-AgNP) to reduce vascular colonization and induce wilt resistance in brassica napus L. Against both fusarium oxysporum and verticillium dahliae. Physiol. Mol. Plant Pathol. 136, 102507. https://doi.org/10.1016/j.pmpp.2024.102507.
Panter, S.N., Jones, D.A., 2002. Age-related resistance to plant pathogens. Adv. Bot. Res 38, 251–280. https://doi.org/10.1016/s0065-2296(02)38032-7.
Parmar, A., Kaur, G., Kapil, S., Sharma, V., Choudhary, M.K., Sharma, S., 2019. Novel biogenic silver nanoparticles as invigorated catalytic and antibacterial tool: a cleaner approach towards environmental remediation and combating bacterial invasion. Mater. Chem. Phys. https://doi.org/10.1016/J.MATCHEMPHYS.2019.121861.
Pieterse, C.M.J., Zamioudis, C., Berendsen, R.L., Weller, D.M., Van Wees, S.C.M., Bakker, P.A.H.M., 2014. Induced systemic resistance by beneficial microbes. Annu Rev. Phytopathol. 52, 347–375. https://doi.org/10.1146/annurev-phyto-082712-102340.
Priya, K., Vijayakumar, M., Janani, B., 2020. Chitosan-mediated synthesis of biogenic silver nanoparticles (AgNPs), nanoparticle characterisation and in vitro assessment of anticancer activity in human hepatocellular carcinoma HepG2 cells. Int. J. Biol. Macromol. https://doi.org/10.1016/J.IJBIOMAC.2020.02.007.
Rashid, S., Islam, S., Qamer, S., et al., 2025. A review of Green synthesized magnesium oxide nanoparticles coated textiles. J. Ind. Text. 55. https://doi.org/10.1177/15280837251313518.
Raza, S., Ansari, A., Siddiqui, N.N., Ibrahim, F., Abro, M.I., Aman, A., 2021. Biosynthesis of silver nanoparticles for the fabrication of non cytotoxic and antibacterial metallic polymer based nanocomposite system. Sci. Rep. 11 (1), 10500. https://doi.org/10.1038/S41598-021-90016-W.
Reinders, M.J., Riemens, M.M., Bremmer, J., 2021. The future of crop protection in Europe. Innov. UK Knowl. Transf. Netw. 44. https://doi.org/10.2861/086545.
Riseh, R.S., Hassanisaadi, M., Vatankhah, M., Babaki, S.A., Barka, E.A., 2022. Chitosan as a potential natural compound to manage plant diseases. Int J. Biol. Macromol. 220, 998–1009. https://doi.org/10.1016/j.ijbiomac.2022.08.109.
Román-Doval, R., Torres-Arellanes, S.P., Tenorio-Barajas, A.Y., Gómez-Sánchez, A., Valencia-Lazcano, A.A., 2023. Chitosan: properties and its application in agriculture in context of molecular weight. Polymers 15 (13), 2867. https://doi.org/10.3390/polym15132867.
Sanguiñedo, P., Fratila, R.M., Estevez, M.B., de la Fuente, J.M., Grazú, V., Alborés, S., 2018. Extracellular biosynthesis of silver nanoparticles using fungi and their antibacterial activity. Nano Biomed. Eng. 10 (2), 165–173. https://doi.org/10.5101/NBE.V10I2.P165-173.
Sanguiñedo, P., Estevez, M.B., Faccio, R., Alborés, S., 2019. Nanopartículas de plata biogénicas a partir del hongo punctularia atropurpurascens para el control de microorganismos. Mundo Nano 12 (22), 101–110. https://doi.org/10.22201/CEIICH.24485691E.2019.22.67627.
Sanguiñedo, P., Faccio, R., Abreo, E., Alborés, S., 2023. Biogenic silver and copper nanoparticles: potential antifungal agents in rice and wheat crops. Chemistry 5 (4), 2104–2119. https://doi.org/10.3390/CHEMISTRY5040143/S1.
Senthilkumar, P., Yaswant, G., Kavitha, S., Chandramohan, E., Kowsalya, G., Vijay, R., Sudhagar, B., Kumar, D.S.R.S., 2019. Preparation and characterization of hybrid chitosan-silver nanoparticles (Chi-Ag NPs); a potential antibacterial agent. Int. J. Biol. Macromol. 141, 290–298. https://doi.org/10.1016/J.IJBIOMAC.2019.08.234.
Shahid-ul-Islam, Butola, B.S., Verma, D., 2019. Facile synthesis of chitosan-silver nanoparticles onto linen for antibacterial activity and free-radical scavenging textiles. Int. J. Biol. Macromol. 133, 1134–1141. https://doi.org/10.1016/J.IJBIOMAC.2019.04.186.
Shams Peykani, L., Farzami Sepehr, M., 2018. Effect of chitosan on antioxidant enzyme activity, proline, and malondialdehyde content in triticum aestivum L. And zea maize L. Under salt stress condition. Iran. J. Plant Physiol. 9 (1), 2661–2670. https://doi.org/10.71551/ijpp.2024.1026145.
Steentjes, M.B.F., Scholten, O.E., van Kan, J.A.L., 2021. Peeling The Onion: towards a better understanding of botrytis diseases of onion. Phytopathology 111 (3), 464–473. https://doi.org/10.1094/PHYTO-06-20-0258-IA.
Sullivan, D.J., Cruz-Romero, M., Collins, T., Cummins, E., Kerry, J.P., Morris, M.A., 2018. Synthesis of monodisperse chitosan nanoparticles. Food Hydrocoll. 83, 355–364. https://doi.org/10.1016/J.FOODHYD.2018.05.010.
Tanović, B., Koščica, M., Hrustić, J., Mihajlović, M., Trkulja, V., Delibašić, G., 2019. Botrytis squamosa - the causal agent of onion leaf blight in Bosnia and Herzegovina. Pestic. i Fitomedicina 34 (1), 9–17. https://doi.org/10.2298/PIF1901009T.
Tharani, S., Bharathi, D., Ranjithkumar, R., 2020. Extracellular Green synthesis of chitosan-silver nanoparticles using lactobacillus reuteri for antibacterial applications. Biocatal. Agric. Biotechnol. 30. https://doi.org/10.1016/j.bcab.2020.101838.
Tian, Y., Che, Z., Sun, D., He, J., Liu, S., Lin, X., 2019. In vitro effects of five different classes of fungicides on growth and development of botrytis cinerea isolated from tree peony in China. HortScience 54 (11), 1984–1988. https://doi.org/10.21273/HORTSCI14431-19.
Vásquez, N., Elizalde, V., Castro, A., Miraballes, I., Pardo, H., Alborés, S., 2024. Development and characterization of chitosan–silver nanohybrids with potential application in the control of fungal phytopathogens. MRS Adv. 9 (2), 113–117. https://doi.org/10.1557/s43580-023-00650-x.
Wang, X., He, M., Wang, X., Liu, S., Luo, L., Zeng, Q., Wu, Y., Zeng, Y., Yang, Z., Sheng, G., Ren, P., Ouyang, H., Jia, R., 2024. Emerging nanochitosan for sustainable agriculture. Int. J. Mol. Sci. 25 (22), 12261. https://doi.org/10.3390/IJMS252212261.
Winayu, I.J., Ekantari, N., Puspita, I.D., Ustadi, Budhijanto, W., Nugraheni, P.S., 2019. The effect of reduced acetic acid concentration on nano-chitosan formulation as fish preservative. IOP Conf. Ser. Mater. Sci. Eng. 633 (1), 012040. https://doi.org/10.1088/1757-899X/633/1/012040.
Zimet, P., Mombrú, Á.W., Faccio, R., Brugnini, G., Miraballes, I., Rufo, C., Pardo, H., 2018. Optimization and characterization of nisin-loaded alginate-chitosan nanoparticles with antimicrobial activity in lean beef. LWT 91, 107–116. https://doi.org/10.1016/J.LWT.2018.01.015.